ARMA 24-154

The Role of Thick Competent Strata in Face Bursting in Underground Longwall Mines

Chambers, D. and Boltz, M.S.
NIOSH/Spokane Mining Research Division, Spokane, WA, USA
Khademian, Z.
NIOSH/Pittsburgh Mining Research Division, Pittsburgh, PA, USA
Walton, G. and Shragge, J.
Colorado School of Mines, Golden, CO, USA

ABSTRACT: Coal bursts are violent dynamic failures that occur in underground coal mines and can injure workers and disrupt mining operations. The coal bursting phenomenon is complex and many factors contribute to a mine's propensity to experience bursting. Among these is the presence of thick competent strata (TCS) in the immediate roof or floor, but how the TCS contribute to bursting is not fully understood. In this work, we created a suite of simple 2D models of a longwall cross section whose stratigraphy is dominated by sandstone. We used these models to explore which TCS parameters influence burst severity and to define a likely failure mechanism. We found that the undermined length of un-caved TCS and properties of the coal-sandstone interface have the greatest effects on a model's burst severity. Interface slip initiated by coal yielding and driven by stored strain energy is the primary failure mechanism. Although real coal bursts are certainly more complex, this work provides insight into a plausible burst mechanism and contributing TCS factors that can guide future research.

1 INTRODUCTION

Coal bursts are violent dynamic failures that occur in underground coal mines. Much like earthquakes, coal bursts are notoriously difficult to predict and can be highly destructive. For example, in the past 40 years, coal bursts have resulted in more than 240 injuries and 20 fatalities in the United States (Iannacchione and Tadolini, 2016). In China, over 300 coal burst related fatalities have occurred since 2006 (Zhang et al., 2017). Many other countries have also experienced coal bursts including Japan, Australia, India, South Africa, Czech Republic, Canada, Germany, and Russia.

Coal bursts are driven mainly by stored strain energy in the coal or nearby strata, or triggered by a pressure wave from a remote source (Gale, 2018). Coal bursts continue to injure workers and disrupt mining operations and, despite research dating back nearly a century (e.g., Rice, 1935), many questions remain about the associated mechanisms and causative factors. For longwall mines, the most productive underground coal mining method, Mark (2016) identified significant seam depth (> 600 m), mining proximity to faults or intrusions, dipping coal beds, multiple seam interaction, and the presence of thick competent strata (TCS) in the immediate (< 15 m) roof or floor as risk factors. Face bursts (coal bursts occurring on the longwall face) have been particularly problematic for many deep mines in the Western United States. For example, between 1983 and 2017 the majority of the 149 bursts reported to the Mine Safety and Health Administration (MSHA) from mines in the state of Utah occurred on the longwall face (Mark, 2018). Severe face bursting has resulted in fatal injuries and even mine closures (Mark, 2016).

A variety of studies have offered explanations on how TCS contribute to bursts in longwall mines. Perhaps the most straightforward is that TCS in the immediate roof can fail to cave for significant distances after seam extraction, effectively forming a cantilever. The cantilever then trans-

fers stress to the coal ahead of the mining face, which can lead to bursting when the peak strength is exceeded (Iannacchione and Tadolini, 2016; Huang et al., 2017). Other research (Cai et al., 2020; Wei et al., 2021; Mark et al., 2012) proposed that sparse jointing systems or faults that traverse the TCS can cause violent failures in the coal. Babcock and Bickel (1984) demonstrated that most coals can burst if confining stresses are rapidly reduced while the principal stress remains high. Iannacchione (1991) modeled this effect and showed that slip on coal interfaces can greatly reduce pillar strength. Moreover, the modeling work of Poeck et al. (2015) showed that softening behavior in the coal and interface both contribute to energy release during coal bursting in a pillar.

A different class of bursting concepts invokes the idea of a remote seismic event causing secondary triggered events or shakedown damage in the workings. These can be caused by slip on a fault or other discontinuity (Bai et al., 2022), brittle sliding of the TCS interface in the overburden (Rice, 1936), failure of TCS above the mined out areas (e.g., Van Dyke et al., 2023; Heasley et al., 2002), and other types of geological failures.

In this work, we explored the mechanisms and TCS-related factors contributing to near-seam coal occurring on the longwall face. After developing an approach for assessing burst susceptibility, we conducted a series of numerical experiments to determine how various TCS features affect a model's bursting severity. Rather than quantify the relationships between parameters, we explored the end members of reasonable ranges to gain intuition about the behavior of the system. We also monitored various parameters of the model as unstable failure progresses to better describe the failure mechanism and process. An improved understanding of the conditions leading to, and dynamics involved in, coal bursting may help guide the selection and deployment of mitigation strategies.

2 MODEL DEVELOPMENT

Following the philosophy of Starfield and Cundall (1988) for modeling data-limited problems, the aim of our numerical experiments was to "gain understanding and explore potential trade-offs and alternatives rather than make absolute predictions." To that end, we selected the simplest models likely to provide insight into the role TCS play in coal bursts occurring on a longwall face. The model components to achieve the minimum level of complexity needed, in our estimation, were:

1. The coal-TCS interface should be able to slip and separate.
2. A TCS-coal interface which allows slip should be modeled explicitly.
3. A TCS cantilever should form behind the longwall.
4. The coal should exhibit strain-softening behavior.
5. The TCS should be much stiffer and stronger than the coal.
6. The TCS in the immediate roof should be able to separate from the rest of the overburden.

We then created a suite of pseudo 2D numerical models which met these requirements. These models were a simplified, version of the mine studied by Chambers and Shragge (2023), which experienced frequent face bursts. In the models, a 600 m deep, 3 m thick coal seam was surrounded by two stiff sandstone units (the TCS). Each TCS in the model had a thickness of 18 m and was surrounded by 30 m of overburden and 18 m of underburden, both of which were also sandstone (Figure 1). The overburden and underburden were included to enable load transfer and to minimize boundary effects on the coal seam. Roller boundary conditions were applied to all sides with the exception of a constant normal stress enforced at the top of the model. The magnitude of the normal stress was calculated to account for the weight of the un-modeled overburden with an assumed density of 2310 kg/m^3. According to Mark and Gadde (2010), most Western U.S. coal mines have a horizontal-to-vertical stress ratio near unity; thus, isotropic in situ stress conditions were assumed.

Material, joint, and interface properties primarily come from the work of Esterhuizen et al. (2010), which provides many useful modeling parameters that were validated against the behavior of both Eastern and Western US coal mines. Despite not having a formal validation procedure in our study, using these material properties provides some assurance the models behaved reasonably. Table 1 shows the coal unconfined compressive strength (UCS) and rockmass properties which used a Hoek-Brown failure criterion (Hoek and Brown, 2019). The rockmass parameters were obtained through numerical calibration rather than classification methods which typically do not work well for coal (Esterhuizen et al., 2010). The values of s and m of the coal rockmass transition linearly over 4% plastic strain to their residual values to provide strain-softening behavior. Because the plasticity of the coal was calibrated for cubic zones with edge lengths of 0.3m, we also used 0.3m cubic zones for the coal seam. The sandstone rockmass was assigned a Young's modulus of 20 GPa, a density of 2,310 kg/m^3, a Poisson's ratio of 0.25, and an elastic constitutive model. Since long model

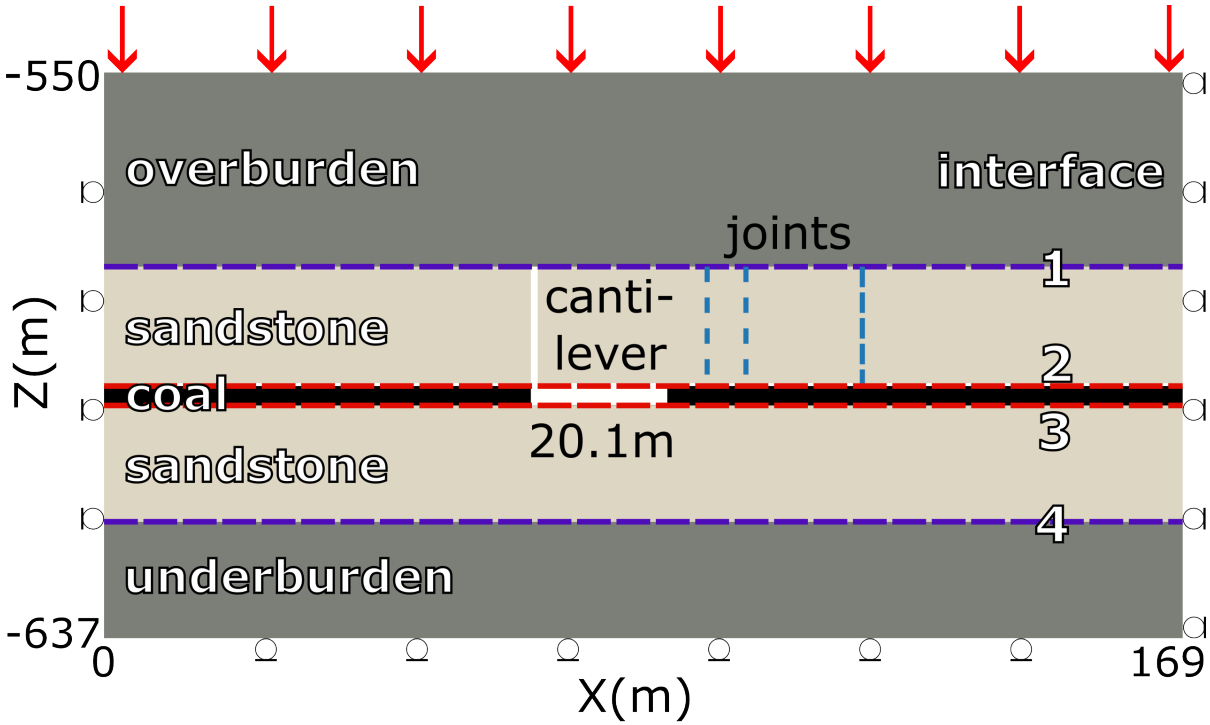

Fig. 1: Panel A shows the geometry of the pseudo 2D model, excavation, and boundary conditions. See text for details.

Table 1: Material properties of coal which follows the Hoek-Brown parameters determined numerically by Esterhuizen et al. (2010). The values of m and s transition linearly over 4% plastic strain to their residual values.

property	value
UCS	20 MPa
Young's modulus	3 GPa
Poisson's ratio	0.25
m-value	1.47
s-value	0.07
m-residual	1.0
s-residual	0.01

run times were not an issue, we also used 0.3m cubic zones for the sandstone units.

FLAC3D discontinuum interfaces were used to simulate three types of features: bedding planes between the sandstone and under/overburden (Figure 1 interfaces 1 and 4), the coal-sandstone interfaces (Figure 1 interfaces 2 and 3), and vertical sandstone joints, which are only inserted into select models as discussed later (Figure 1 vertical dashed blue lines). The interface between the overburden and the top TCS (interface 1) allows the TCS to separate from the overburden, which likely occurs in real mines as TCS cantilevers sag. As mentioned earlier, interfaces 2 and 3, which are in contact with the coal, play an important mechanistic role in coal bursting. Table 2 shows interface properties, all of which follow the Mohr Coulomb slip criterion. The coal interface properties and the sandstone bedding-plane strength properties were selected from the range provided by Esterhuizen et al. (2010) that matched the closest UCS to tested samples from the mine mentioned by Chambers and Shragge (2023). The shear and normal stiffness of the sandstone bedding plane were set equal to those of the coal interface.

Most models included a 20.1 m cantilever, which is within the range of un-caved TCS observed at the mine on which the model is based. Although TCS cantilevers of this length may not be typical for most longwall mines, some have reported lengths of up to 45 m (Akinkugbe et al., 2007). The TCS cantilevers were developed using the following procedure. First, the unexcavated model was brought to equilibrium under gravity loading using an average mechanical ratio ($\overline{M}$, see Section 8) of 1e-5. Then, a vertical slot was created in the top TCS to reduce the amount of load transmitted to the left coal pillar and thereby simulate a caving situation in which the TCS breaks in discrete blocks behind the longwall. We assumed that broken TCS would have no effect on the current TCS cantilever and therefore no consideration was made for gob compaction response under caving loads. The model was again run until the same equilibrium criterion was met. Next, a series of 3m excavation steps were performed using FLAC3D's *zone relax excavate* command. This command gradually reduces stiffness, density,

Table 2: Model interface properties which come from Esterhuizen et al. (2010). In the base model, interfaces 1 and 4 were assigned properties of the "sandstone" column and interfaces 2 and 3 were assigned properties of the "coal interface" column. Properties in other columns were used by models discussed in Section 4.

	Coal interface	Sandstone weak	Sandstone	Sandstone strong	Shale
Normal stiffness (GPa/m)	100	100	100	100	100
Shear stiffness (GPa/m)	50	50	50	50	50
Friction angle (deg)	25	20	25	30	5
Cohesion (MPa)	0.1	3.35	4.53	8.11	0.10
Tensile strength (MPa)	0	0	0.35	5.57	0.03

and normal forces of the excavated volume to minimize artificial damage to surrounding zones from sudden removal and to suppress dynamic behavior (Itasca Consulting Group, Inc., 2023). Once the TCS cantilever was fully formed, the burst-susceptibility of the model was evaluated. All models used large strain mode, which allows the position of zones to change as deformation occurs.

3 MODEL EVALUATION

No consensus exists on the best way to quantify the occurrence and severity of rock/coal bursts in a numerical model, and many different approaches appear in the literature. Perhaps the most popular of these appeal to energy concepts and use metrics such as total dissipated energy (Khademian and Ugur, 2018), energy release rate (Sears and Heasley, 2009), total or change in stored elastic energy (Jiang et al., 2010; Kim et al., 2018), and total plastic work (Wang and Kaunda, 2019). Other strategies appeal to physical properties of the model such as local mine stiffness (Raja et al., 2018), effective thickness of TCS units after yield (Lawson et al., 2017), or maximum velocity of the mine workings' surface (Zhang et al., 2021).

We selected two metrics to quantify the burst-susceptibility and severity: peak particle, or grid point, velocity (PPV) and maximum rate of plastic work ($\dot{W}_{p\,max}$) near the mining face. Since we are interested in investigating face bursts characterized by significant particle velocities, violent dynamic fracturing, and ejection of the coal face, PPV is a reasonable metric because a large PPV is a necessary physical characteristic of this phenomenon and is often used as a proxy for burst damage (e.g., Potvin and Wesseloo, 2013). FLAC3D uses a finite-volume scheme to explicitly step through simulation time and numerically solve the equations of motion, so grid point velocities can be recorded in discrete model time steps. However, there are some subtleties that prevent the numerical model from producing realistic face burst PPV estimates. Primarily, FLAC3D is a continuum-based modeling software and cannot simulate complex fracturing, particle ejection, and zone separation that occur in actual face bursts. However, the rate of plastic dissipated work ($\dot{W}_p$), which is the energy directed towards causing non-recoverable damage in the rockmass, could be a useful proxy because higher $\dot{W}_p$ are indicative of more violent failure than lower $\dot{W}_p$ (Wang and Kaunda, 2019). Therefore, as long as all models use the same coal constitutive model, which controls plastic work accumulation behavior, a model with a greater ($\dot{W}_{p\,max}$) has a higher potential of violent fracture and ejection than the model with a lower value. The second reason FLAC3D fails to produce realistic velocities is its damping implementation (see Section 8). Essentially, FLAC3D dissipates kinetic energy from the model every cycle to converge on a static solution. The default energy damping scheme is efficient for reaching equilibrium quickly but does not imitate energy damping in real geological systems well. However, because all models are subject to these conditions, PPV is useful as a strictly *comparative* metric.

We used the following procedure to calculate PPV, $\dot{W}_p$, and other parameters useful for interpreting model results. First, we issued the FLAC3D *zone relax* command mentioned earlier to indicate the 3m of coal to the right of the mining face should be removed. However, rather than use the default servo-controlled option that attempts to adjust extraction rates to suppress dynamic behavior, we reduced the density and stiffness of the extracted zones linearly over the span of 2,000 time steps (a.k.a. cycles) using the *cycle* option. Next, the model was run until both the coal extraction completed and a $\overline{M}$ of 2e-5 was reached. Every 20 cycles while the model was running, we recorded the following data for all coal *zones*: the complete stress and strain tensors, the current centroid location of the zone, the accumulated plastic work, and the stored elastic energy. We also recorded the following information for all coal *grid points*: current position, current velocity, current acceleration, and equivalent mass. We then calculate V_{max} by taking the maximum grid point velocity recorded in the first 3 m of coal next to the mining face, which forms a velocity time series. PPV, then, is just the maximum value

of V_{max}. $\dot{W}_p$ is calculated by averaging the accumulated plastic work over all the zones in the first 3 m of coal for each recorded time step, then taking the two point forward difference to calculate rate per cycle. $\dot{W}_{p\,max}$ is the maximum value of the time series $\dot{W}_p$. While 3.0 m is a partially arbitrary choice, it is a reasonable estimate for depth of material affected by typical bursts (Gale, 2018). Additionally, we found several other zone and interface metrics useful to understand a model's behavior. The zone metrics included vertical stress and accumulated plastic work averaged over coal zones with the same initial X position (i.e., vertical slices). The interface metrics included shear stress and slip along the top interface.

4 RESULTS

4.1. Influence of Cantilever Length

As cantilever length increased, the maximum vertical and shear stress in front of the mining face also increased (Figure 2 A and B). Additionally, the peak values moved further into the coal block as the coal zones near the face yield. The peak in normal stress near the face causes increased resistance to slip along the coal interface and thus higher interface shear stress and lower interface slip overall (Figure 2 C and D). The burst metrics $\dot{W}_{p\,max}$ and PPV both increase for increasing cantilever length.

4.2. Influence of Upper Bedding Plane

The moderate strength sandstone upper bedding plane (interface 1) of the base model was substituted with a stronger sandstone bedding plane and then a thin, weak shale layer to test two reasonable end members of interface strength. Properties for these interfaces are shown in Table 2 in columns "strong sandstone" and "shale," respectively. Increasing the bedding plane strength had a negligible effect in all measured aspects (Figure 3). This is because the interface in the base model remained largely intact; examining the model in the FLAC3D interface revealed that only 3 m of the interface failed in tension and 10 m slipped in shear. In other words, using a stronger interface has little effect because it largely remained intact using the base properties.

When interface 1 was replaced with a weak shale layer, however, the peak vertical and shear stress of the coal, as well as the yielded coal volume (Figure 3 B), increased. This occurred because the interface lost tensile strength and was not able to transfer the TCS cantilever load to the overburden. Interestingly, the displacement along the entire upper coal interface nearly doubled from 1.5 cm to 3.0 cm and the shear stress at face distances greater than 5 m also nearly doubled, but remained unchanged for lesser values (Figure 3 C and D). The increase in shear stress on the coal interface to the right of the yielded coal volume occurred because interface 1 no longer provided much shear resistance against the TCS elastically unloading into the vertical slot, so more shear stress was transferred to the coal interface (interface 2). Interestingly, weakening interface 1 does not have a large effect on the burst metrics, although $\dot{W}_{p\,max}$ does increase slightly, perhaps due to the increased loading weight.

4.3. Influence of Coal Interface

Since the coal interface plays an important role in coal bursting, we varied several parameters to gain insight into their effects, starting with the interface cohesion. Using the default friction angle of 25°, test cases were created for weak cohesion (0 MPa) and strong cohesion (1.0 MPa), with the base model (0.1 MPa) included for reference (Figure 4). These cohesion ranges were suggested by Iannacchione (1991). Increasing the cohesion tenfold from the base model had little effect on most measured parameters, but the interface slip decreased and the bursting metrics increased significantly (Figure 4 C, E and F). The base and zero cohesion models did not vary as drastically, which could be due to the smaller differences in their cohesion.

Increasing the friction angle from the base case of 25° to 30° decreased the slip along the interface and increased the burst metrics by 20-40% (Figure 5). A drastic drop in friction angle from 25° to 10°, the lower limit suggested by Iannacchione (1991), significantly affected every measured metric. The peak vertical and shear stress moved further into the pillar, and the maximum slip magnitude along the interface more than tripled. The velocity and plastic work rate had much smaller peaks but remained elevated longer (Figure 5), indicating a less dynamic but larger duration ground reaction.

We also tested the effect of residual interface parameters, which replace the initial parameters after the interface slips and can be used to introduce shear-softening behavior. We explored applying residual values (i.e. deviating from the "perfectly plastic" base model condition) for three scenarios: only reducing cohesion (dropping from 0.1 MPa to 0.0 MPa), only reducing friction angle (dropping from 25° to 10°), and a model which dropped both cohesion and friction angle (Figure 6). The only effect of the residual cohesion drop was to slightly lower the bursting metrics. Introduction of a reduced residual friction angle, however, had a much larger effect. The vertical and principal shear stress, as well as the interface slip and $\dot{W}_{p\,max}$, were similar to those of the model with lower peak friction angle (Figure 5). Figure 6 E shows the lower residual friction angle caused a series of high veloc-

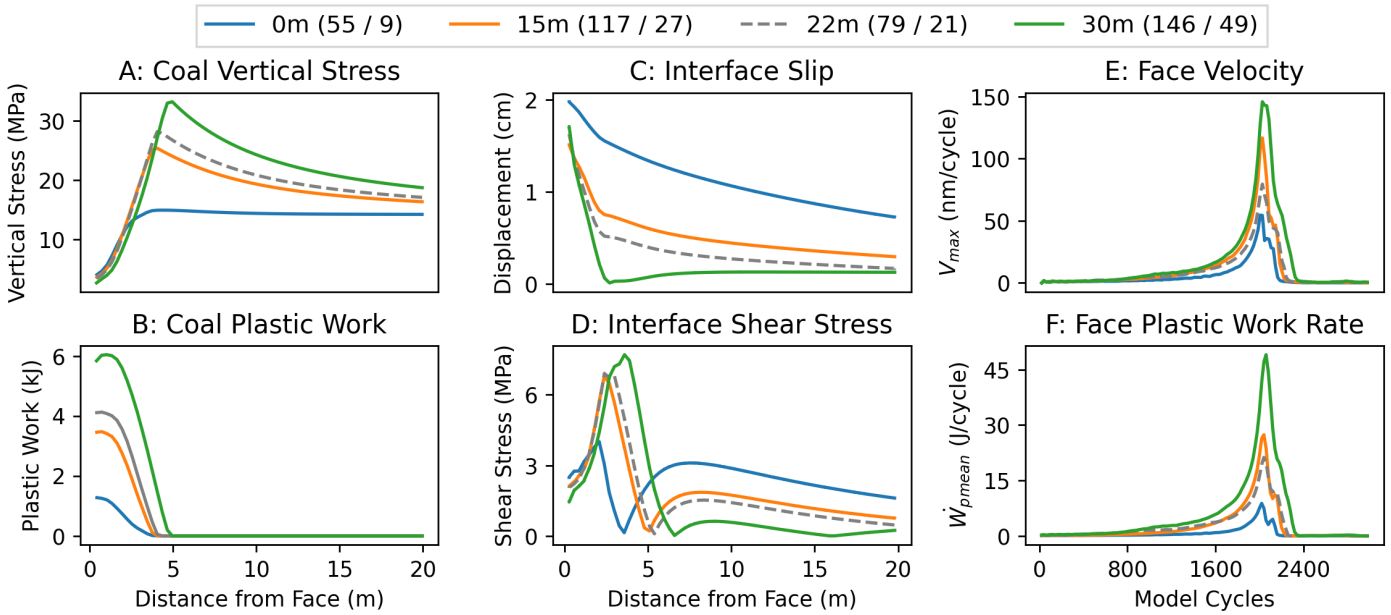

Fig. 2: Model results for varying TCS cantilever length. Panels A and B show the vertical stress and dissipated plastic energy, respectively, averaged over vertical slices of the coal zones. The x value in which a plastic work curve reaches zero in panel B indicates the limit of the yielded coal volume. Panels C and D show the shear displacement and shear stress on the upper coal-sandstone interface. Panel E shows the maximum velocity of all grid points in the first 3 m of coal as a function of model time, and panel F shows the average rate of plastic work for the same volume, also as a function of model time. The numbers in parenthesis next to the color labels are the burst metrics, with the first being the peak velocity value (PPV) from panel E with unit of nm/cycle and the second the maximum rate of plastic work ($\dot{W}_{p_{max}}$) from panel F with units of J/cycle. The dotted grey line in this and subsequent figures indicates the base model.

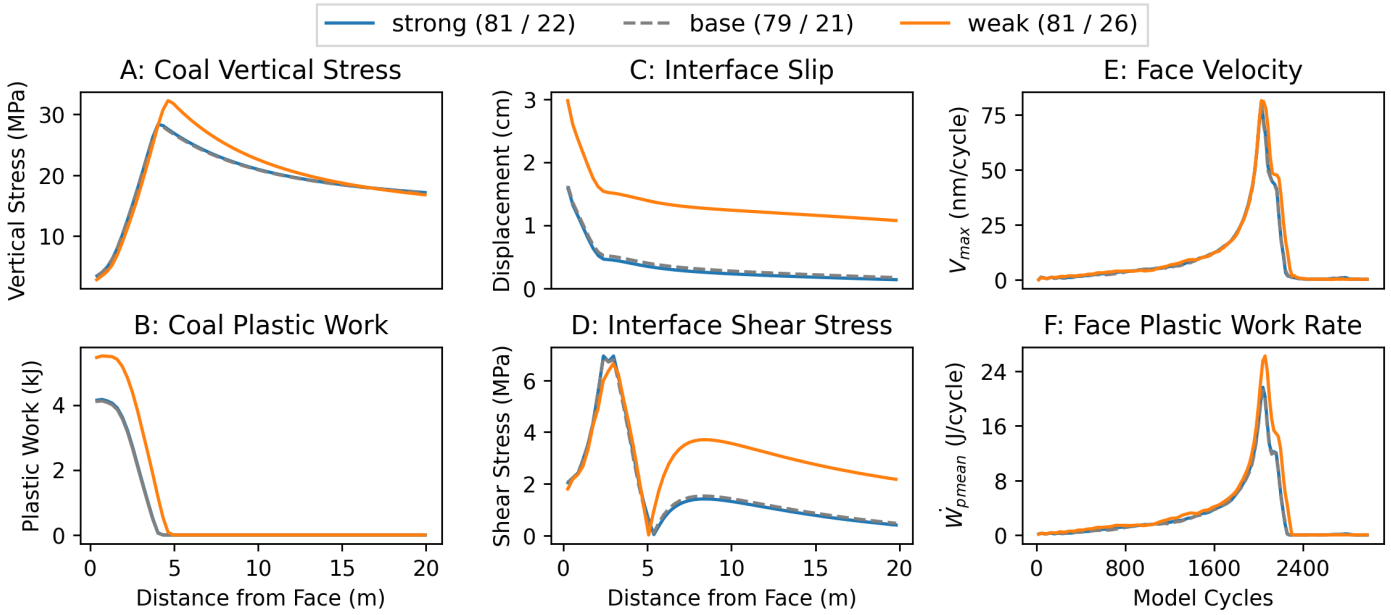

Fig. 3: Model results for varying interface 1 properties from the base values shown in Table 2 to weaker values representative of a thin shale layer. See Figure 2 for an explanation of each panel.

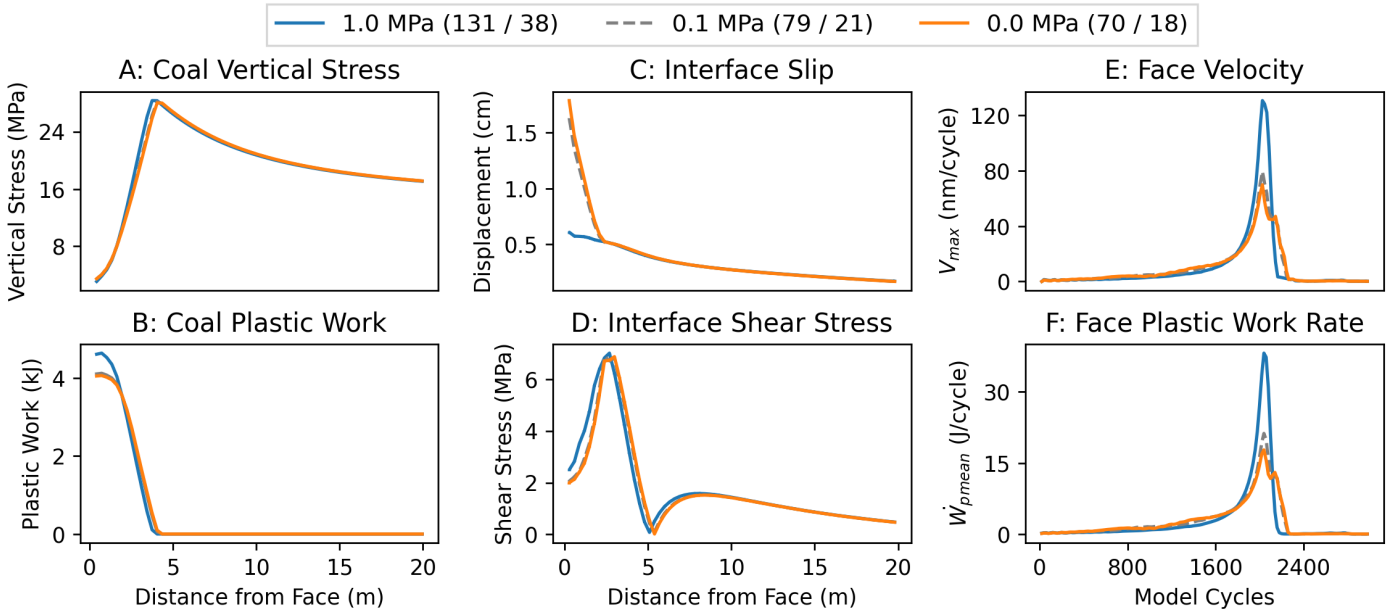

Fig. 4: Model results for varying coal interface cohesion. See Figure 2 for an explanation of each panel.

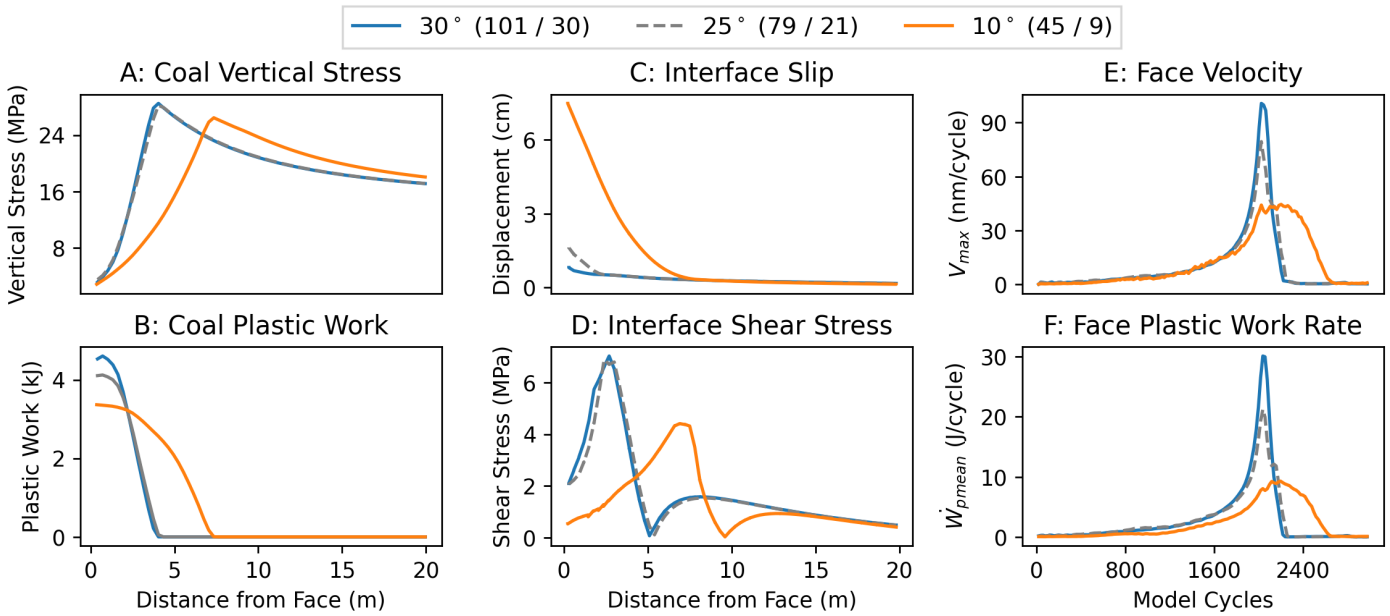

Fig. 5: Model results for varying coal interface friction angle. See Figure 2 for an explanation of each panel.

ity spikes during the extraction sequence. Each of these could represent an unstable failure, though peak velocities are still 30% lower than the PPV of the base model.

4.4. Influence of Vertical Joints

The final set of models included a single vertical joint in the TCS at varying distances (6 m, 12 m, 30 m) ahead of the face, labeled as "near,", "mid," and "far," on Figure 7. The joint properties are listed in Table 2 as “sandstone weak,” which come from Esterhuizen et al. (2010), except the tensile strength is set to 0 MPa. Since the bedding planes were quite strong in the base model, the joints had a negligible effect on any of the measured parameters. However, in order to measure some effect from the vertical joints, we assumed interface 1 to be a thin shale layer, in which case the joints did have an effect (Figure 7). Specifically, the middle and far joint cases increase vertical stress, interface displacement, and the bursting metrics from the base case. Compared to the other models with joints, the near joint case did increase interface slip and PPV, but not $\dot{W}_{pmax}$.

5 DISCUSSION

The face bursting mechanism revealed through this modeling exercise has two related components: (1) a concentrated area of high shear stress on the coal interface, and (2) an adjacent concentration of stored elastic energy in the coal. Consider Figure 8, which shows the 30 m cantilever case from Section 4.1 as extraction progressed through model cycles (vertical axes, bottom to top). At time step 2000, when the block in front of the mining face was fully extracted, we note the following observations: the normal and shear stress on the interface shifted (panels A and B), the interface slipped about 2 cm (panel C), a new yield zone formed (panel D), the elastic energy concentration abruptly shifted (Panel E), and a burst of kinetic energy was released (panel F). The face distance of the peak interface shear stress corresponds to a region of partially yielded coal. This can be seen by comparing the face distance location of the peak shear stress band in panel B with the total plastic work in panel D. The peak elastic energy, however, was located to the right of the yield region and provides the driving force for the interface failure.

The concentration of shear stress and stored elastic energy arose because the large stiffness contrast between the TCS and coal enables localized strain energy accumulation in the coal seam, and the TCS cantilever induced a non-uniform vertical loading on the coal block. As the cantilever length increased, the stress distribution becomes more prone to concentrated high-energy slip, as seen in Figure 2. This is apparent because increasing cantilever length not only caused an increase in peak vertical stress, but also an increase in the difference between the peak and background values. At larger cantilever lengths, this vertical stress concentration created a locked portion of the interface that experienced little displacement and was subjected to significant shear stress (Figure 2 A,C,D). When the strength of the coal was reduced by dropping confinement through extraction of material the released strain energy concentrated near the locked section of the interface manifested as a coal burst with a significant interface shear stress drop. Essentially, this is the “loss of confinement” mechanism described by Iannacchione and Tadolini (2016), because it is a loss of confinement on a highly stressed volume of un-yielded coal that drives the failure. However, apart from extraction-related loss of confinement, the failure could also be triggered by increased vertical stress in the coal. Additionally, the term “loss of confinement” only describes the conditions leading to failure, not the nature of the failure itself. Therefore, strain-induced interface slip, or strain-slip, might be a better term for the mechanism observed in our models.

Clearly, the coal interface plays an extremely important role and there are several insights gained from varying interface properties. First, increasing the cohesion of the interface led to significantly higher burst metrics but, apart from reducing slip on the interface near the immediate face, changes in other parameters were negligible (Figure 4). Decreasing the friction angle, however, significantly reduced the maxima of these metrics and shifted the the peak location into the coal block, indicating a larger yielded volume (and much larger slipped interface area). Increasing friction angle increased the burst metrics, and lowering friction angle significantly reduced them. Therefore, for the cases involving perfectly plastic interface behavior, higher strength interfaces (in terms of friction angle and cohesion) have more severe coal bursting than weaker interfaces. Considering interfaces which exhibit shear weakening, the model with a zero residual cohesion and the zero cohesion model behaved identically. The models with low peak friction angle and low residual friction angle also behaved similarly, but the residual drop in friction angle creates velocity spikes reminiscent of stick-slip earthquake behavior (Brace and Byerlee, 1966). Based on these two results, we infer the yielded (slipped) portions of the interface primarily control models behavior for the measured metrics, but this could be different if alternate coal constitutive models were used. Moreover, more complex interface shear softening models could exhibit different behavior.

The suite of models incorporating vertical joints only showed slight variations from the base model. However,

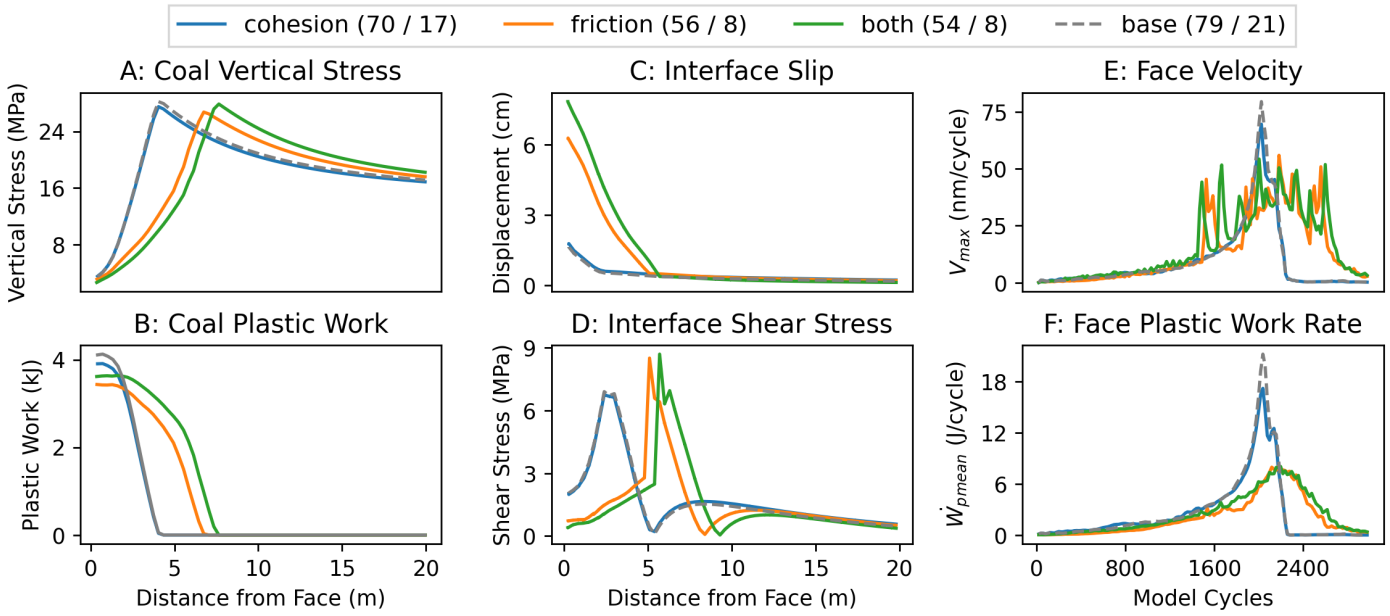

Fig. 6: Model results for varying coal interface residual strength. The cohesion values were reduced from 0.1 MPa to 0.0 MPa and friction angles were reduced from 25° to 10°. See Figure 2 for an explanation of each panel.

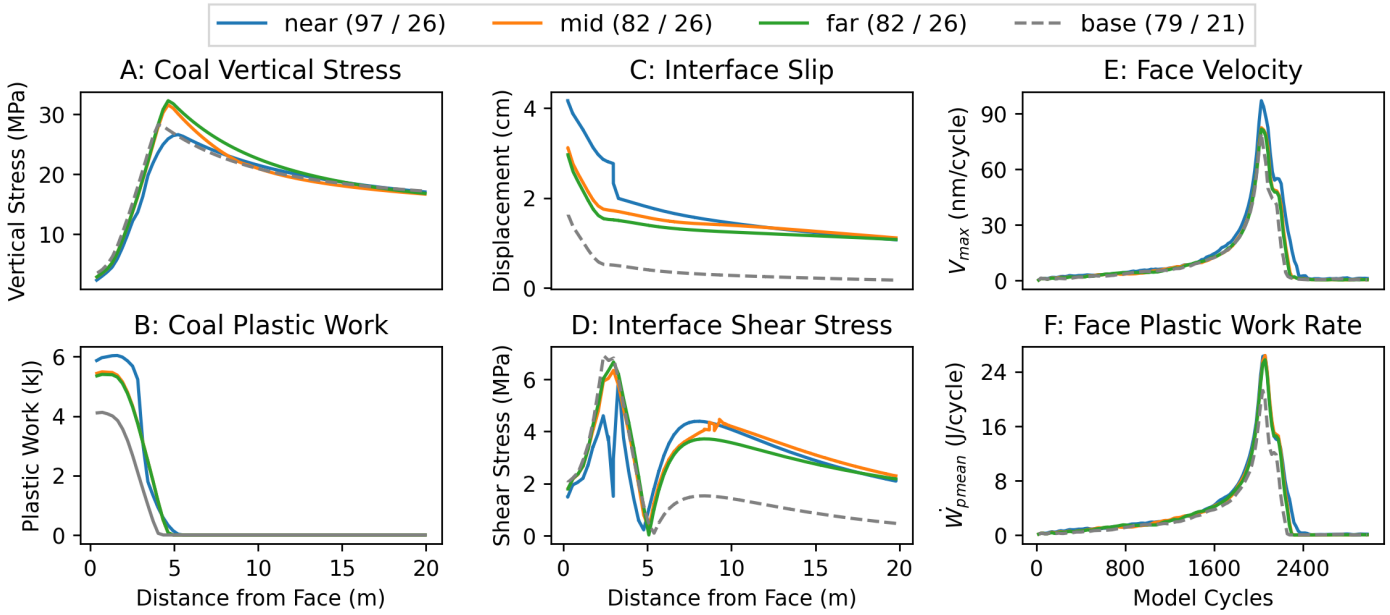

Fig. 7: Model results for vertical joints in the TCS for joints 6m (near), 12m (mid) and 30m (far) from the working face. See Figure 2 for an explanation of each panel.

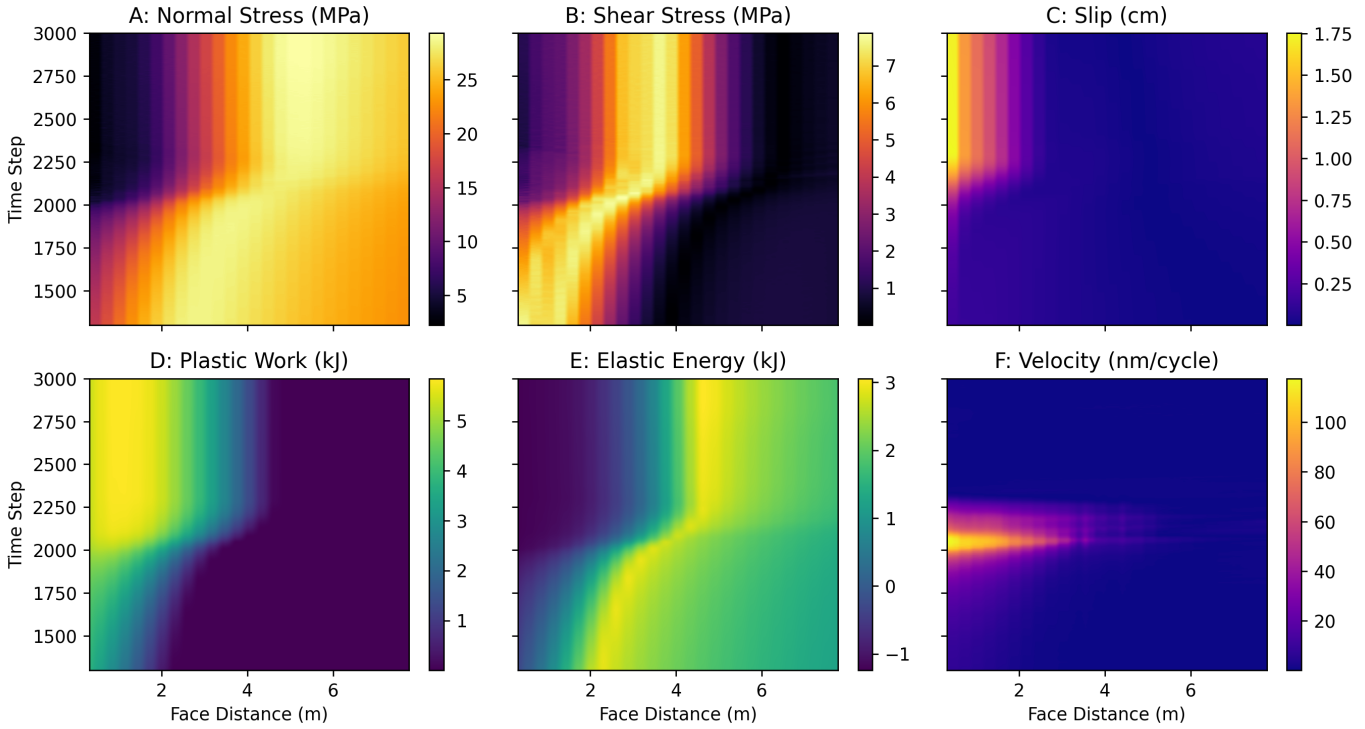

Fig. 8: Dynamic evolution of interface normal stress (A), interface shear stress (B), interface slip (C), average plastic work in the coal block (D), average stored elastic energy in the coal (E), and grid point velocity of the coal zones (F) as a function of face distance (x axis) and model time steps (Y axis).

since the location of the joint, joint properties, and properties of interface 1 can be highly variable, there is likely a wide range of unexplored possible behavior. Therefore, vertical joints could play a much larger role in coal bursting outside of the parameters we explored in this study.

There are several aspects of this work that can be improved. First, the models did not account for the longwall shields, although they certainly have an effect on the face behavior (e.g., Bai et al., 2014; Islavath, 2023). Explicitly modeling the shields, or simply accounting for their support pressure, could improve the accuracy of the models. We would also like to simulate more realistic TCS behavior, perhaps by using a Hoek-Brown failure criterion as was done by Newman and Newman (2023) and implicitly accounting for gob formation (when caving is detected) as in Esterhuizen et al. (2010). Including more realistic geology as well extending the model to three dimensions to account for stress transfer from previously mined areas could increase model realism.

We also did not explore any failure modes which involve dynamic effects, such as sudden breaking of TCS behind or above the longwall. In our estimation, it seems unlikely that a dynamic stress wave itself would lead directly to the concentrated face burst events we targeted in this study, but it might be possible that a dynamic stress wave could affect the coal interface enough to trigger the release of stored elastic energy in the seam. Additional research, which necessarily includes fully dynamic modeling, may shed light on these more complex failure mechanisms. Moreover, geophysical measurements, especially from emerging high resolution methods such as distributed fiber-optic sensing, could help elucidate coal burst failure mechanisms.

6 CONCLUSIONS

By developing simple 2D models, we explored the effects of several TCS factors which influence coal bursting on a longwall face. We observed a strain driven interface slip mechanism in which yielding in one section of the coal causes slip along the interface, associated loss of confinement, and subsequent rapid release of stored elastic energy. The potency of the failure depends on several factors, but increasing cantilever length, and the associated magnitude and heterogeneity of loading on the coal was the most significant in our models. Additionally, interface cohesion and friction have substantial impacts over the tested ranges. Vertical jointing did not have a major impact, but it could have a larger effect outside of the small parameter space we explored. The insight from this and future work may help guide the design and implemen-

tation of coal burst mitigation strategies.

7 DISCLAIMER

The findings and conclusions in this report are those of the author(s) and do not necessarily represent the official position of the National Institute for Occupational Safety and Health, Centers for Disease Control and Prevention. Mention of any company or product does not constitute endorsement by NIOSH, CDC.

8 APPENDIX A: FLAC3D BACKGROUND

FLAC3D is a popular program for simulating a wide variety of geomechanical systems (Itasca Consulting Group, Inc., 2023). It uses an explicit finite-volume scheme to solve the equations of motions. Essentially, this means the program iterates over time steps (cycles) and updates the model state until a user-defined stopping criterion is reached. Because time steps are small, complex non-linear constitutive models can be accurately implemented. In terms of each grid point in the model, Newton's second law can be described as:

$$F_i = M\left(\frac{dv_i}{dt}\right), \tag{1}$$

where F_i is the unbalanced force, M is the node's equivalent mass, and v is nodal velocity. Index i indicates the principal directions ($i = 1, 2, 3$).

To converge to a static solution, energy must be removed from the system as the simulation progresses. By default, FLAC3D uses "local non-viscous" damping, which adds a damping force, $F_{(i)}$, to Equation 1:

$$F_i + F_{(i)} = M\left(\frac{dv_i}{dt}\right), \tag{2}$$

where $F_{(i)}$ is defined as

$$F_{(i)} = -\alpha |F_i| sgn(v_i), \tag{3}$$

parameter α is a scalar constant with a default value of 0.8, $|F_i|$ indicates the absolute value of F_i and sgn is an operator which returns the sign of the input. There are two important consequences of Equation 3. First, kinetic energy is only damped when unbalanced forces exist. Second, the magnitude of the damping force is proportional to the amplitude of the current unbalanced force (F_i), but with a direction opposite (in sign) to that of the current velocity vector (v_i).

The default criterion to determine when a model has converged (i.e., reached equilibrium) is when the mean mechanical ratio ($\overline{M}$), which is a ratio of unbalanced to balanced forces, drops below a specified threshold (1e-5 by default):

$$\overline{M} = \frac{\sum_{j=1}^{n} < \sum_i f_i >}{\sum_{j=1}^{n} \sum_i < f_i >} \tag{4}$$

where j is a summation index over all nodes n, i is a summation index over the principal directions, and <> is the Manhattan distance operator defined as:

$$< f_i >= \sum_i |f_i| \tag{5}$$

REFERENCES

1. Akinkugbe, Y., Su, D., Hasenfus, G., Morris, T. J., and Fisher, B. (2007). The roof behavior of a longwall tailgate under massive sandstone strata. *26th International Conference on Ground Control in Mining*.

2. Babcock, C. O. and Bickel, D. L. (1984). Constraint - the missing variable in the coal burst problem. In *ARMA US Rock Mechanics/Geomechanics Symposium*. American Rock Mechanics Association.

3. Bai, J., Dou, L., Li, J., Zhou, K., Cao, J., and Kan, J. (2022). Mechanism of coal burst triggered by Mining-Induced fault slip under High-Stress conditions: A case study. *Front Earth Sci. Chin.*, 10.

4. Bai, Q.-S., Tu, S.-H., Zhang, X.-G., Zhang, C., and Yuan, Y. (2014). Numerical modeling on brittle failure of coal wall in longwall face—a case study. *Arab. J. Geosci.*, 7(12):5067–5080.

5. Brace, W. F. and Byerlee, J. D. (1966). Stick-slip as a mechanism for earthquakes. *Science*, 153(3739):990–992.

6. Cai, W., Dou, L., Si, G., and Hu, Y. (2020). Fault-induced coal burst mechanism under mining-induced static and dynamic stresses. *Proc. Est. Acad. Sci. Eng.*, 7(5):687–700.

7. Chambers, D. and Shragge, J. (2023). Seismoacoustic monitoring of a longwall face using distributed acoustic sensing. *Bull. Seismol. Soc. Am.*, 113(4):1652–1663.

8. Esterhuizen, E., Mark, C., and Murphy, M. (2010). Numerical model calibration for simulating coal pillars, gob and overburden response. In *Proceedings of the 29th International Conference on Ground Control in Mining*, pages 46–57.

9. Gale, W. J. (2018). A review of energy associated with coal bursts. *International Journal of Mining Science and Technology*, 28(5):755–761.

10. Heasley, K. A., Ellenberger, J. L., and Jeran, P. W. (2002). Microseismic activity associated with a deep longwall coal mine. In *SME Annual Meeting*. Society for Mining, Metallurgy, and Exploration.

11. Hoek and Brown (2019). The Hoek–Brown failure criterion and GSI–2018 edition. *J. rock mech. geotech. eng.*, 11(3):445–463.

12. Huang, B., Chen, S., and Zhao, X. (2017). Hydraulic fracturing stress transfer methods to control the strong strata behaviours in gob-side gateroads of longwall mines. *Arabian Journal of Geosciences*, 10(11):236.

13. Iannacchione, A. (1991). Effects of roof and floor interface slip on coal pillar behavior. *Int. J. Rock Mech. Min. Sci. Geomech. Abstr.*, 28(2-3):A186–A187.

14. Iannacchione, A. T. and Tadolini, S. C. (2016). Occurrence, predication, and control of coal burst events in the U.S. *International Journal of Mining Science and Technology*, 26(1):39–46.

15. Islavath, S. R. (2023). Numerical modelling approach for estimation of a yield zone in the face of a deep longwall panel. *Sci. Rep.*, 13(1):20811.

16. Itasca Consulting Group, Inc. (2023). Fast lagrangian analysis of continua.

17. Jiang, Q., Feng, X.-T., Xiang, T.-B., and Su, G.-S. (2010). Rockburst characteristics and numerical simulation based on a new energy index: a case study of a tunnel at 2,500 m depth. *Bull. Eng. Geol. Environ.*, 69(3):381–388.

18. Khademian, Z. and Ugur, O. (2018). Computational framework for simulating rock burst in shear and compression. *Int. J. Rock Mech. Min. Sci.*, 110:279–290.

19. Kim, B.-H., Larson, M. K., and Lawson, H. E. (2018). Applying robust design to study the effects of stratigraphic characteristics on brittle failure and bump potential in a coal mine. *Int J Min Sci Technol*, 28(1):137–144.

20. Lawson, H. E., Tesarik, D., Larson, M. K., and Abraham, H. (2017). Effects of overburden characteristics on dynamic failure in underground coal mining. *International Journal of Mining Science and Technology*, 27(1):121–129.

21. Mark, C. (2016). Coal bursts in the deep longwall mines of the united states. *International Journal of Coal Science & Technology*, 3(1):1–9.

22. Mark, C. (2018). Coal bursts that occur during development: A rock mechanics enigma. *International Journal of Mining Science and Technology*, 28(1):35–42.

23. Mark, C. and Gadde, M. (2010). Global trends in coal mine horizontal stress measurements. In Aziz, N. and Kininmonth, B., editors, *Proceedings of the 2010 Coal Operators' Conference*, Resource Operators Conference. ro.uow.edu.au.

24. Mark, C., Phillipson, S. E., Tyrna, P., and Gauna, M. (2012). Characteristics of coal bursts in the north fork valley of the gunnison river, colorado. In *Proceedings of the 30th international conference on ground control in mining.*, pages 1–12.

25. Newman, C. and Newman, D. (2023). Gate road layout for Deep-Cover, dipping longwall recovery: A case study in the western united states. In *42nd International Conference on Ground Control in Mining*.

26. Poeck, E., Zhang, K., Garvey, R., and Ozbay, U. (2015). Energy concepts in the analysis of unstable coal pillar failures. In *34th international conference on ground control in mining*, pages 8–13.

27. Potvin, Y. and Wesseloo, J. (2013). Keynote lecture: Improving seismic risk management in hardrock mines. In *proceedings of the 8th International Symposium on Rockbursts and Seismicity in Mines (Rasim8)*. academia.edu.

28. Raja, S., Mandal, P. K., Paul, P. S., and Das, A. J. (2018). Prediction of coal bump with respect to local mine stiffness and post-failure stiffness using numerical modelling. *J. Mines Met. Fuels*, 66(6):328–338.

29. Rice, G. S. (1935). *Bumps in Coal Mines of the Cumberland Field, Kentucky and Virginia: Causes and Remedy*. United States Bureau of Mines.

30. Rice, G. S. (1936). Bumps in coal mines—theories of causes and suggested means of prevention or of minimizing effects. *Transactions of the American Institute of Mining and*.

31. Sears, M. and Heasley, K. (2009). An application of energy release rate. In *Proceedings of the 28th International Conference on Ground Control in Mining*, pages 10–17.

32. Starfield, A. M. and Cundall, P. A. (1988). Towards a methodology for rock mechanics modelling. *International Journal of Rock Mechanics and Mining Sciences & Geomechanics Abstracts*, 25(3):99–106.

33. Van Dyke, M., Klemetti, T., Khademian, Z., Wickline, J., and Beale, J. (2023). Evaluation of seismic potential in a longwall mine with massive sandstone roof under deep overburden: an update. *Mining, Metallurgy & Exploration*.

34. Wang, F. and Kaunda, R. (2019). Assessment of rockburst hazard by quantifying the consequence with plastic strain work and released energy in numerical models. *International Journal of Mining Science and Technology*, 29(1):93–97.

35. Wei, C., Zhang, C., Canbulat, I., and Huang, W. (2021). Numerical investigation into impacts of major fault on coal burst in longwall mining – a case study. *Int. J. Rock Mech. Min. Sci.*, 147:104907.

36. Zhang, C., Canbulat, I., Hebblewhite, B., and Ward, C. R. (2017). Assessing coal burst phenomena in mining and insights into directions for future research. *International Journal of Coal Geology*, 179:28–44.

37. Zhang, W., Ma, N., Ren, J., and Li, C. (2021). Peak particle velocity of vibration events in underground coal mine and their caused stress increment. *Measurement*, 169:108520.